

Cell tracking of convective rainfall: sensitivity of climate-change signal to tracking algorithm and cell definition

Edmund P. Meredith*

Institut für Meteorologie, Freie Universität Berlin, Germany
`edmund.meredith@met.fu-berlin.de`

Uwe Ulbrich

Institut für Meteorologie, Freie Universität Berlin, Germany

Henning W. Rust

Institut für Meteorologie, Freie Universität Berlin, Germany

Abstract

Contains supporting figures and discussion.

1 Supporting Figures

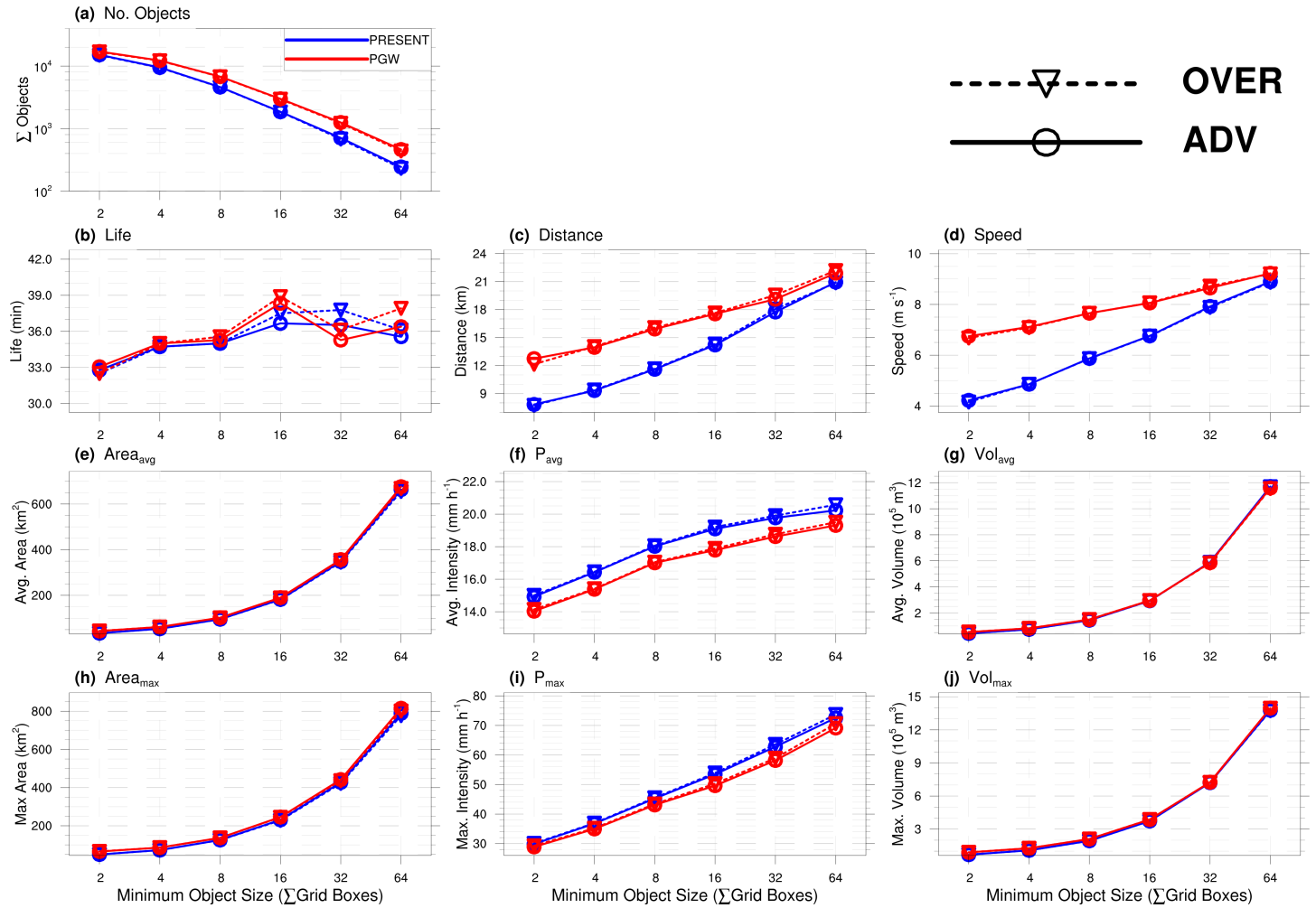


Figure S1: Different object properties in present and future climates as a function of the object's minimum-area criterion A_{\min} , for both algorithms. These are the absolute values underlying the change signals shown in Fig. 3 of the main manuscript. A_{\min} is defined in terms of grid boxes, with each grid box having an area of $\sim 7.7 \text{ km}^2$. The A_{\min} range thus spans approximately 15 to 493 km^2 .

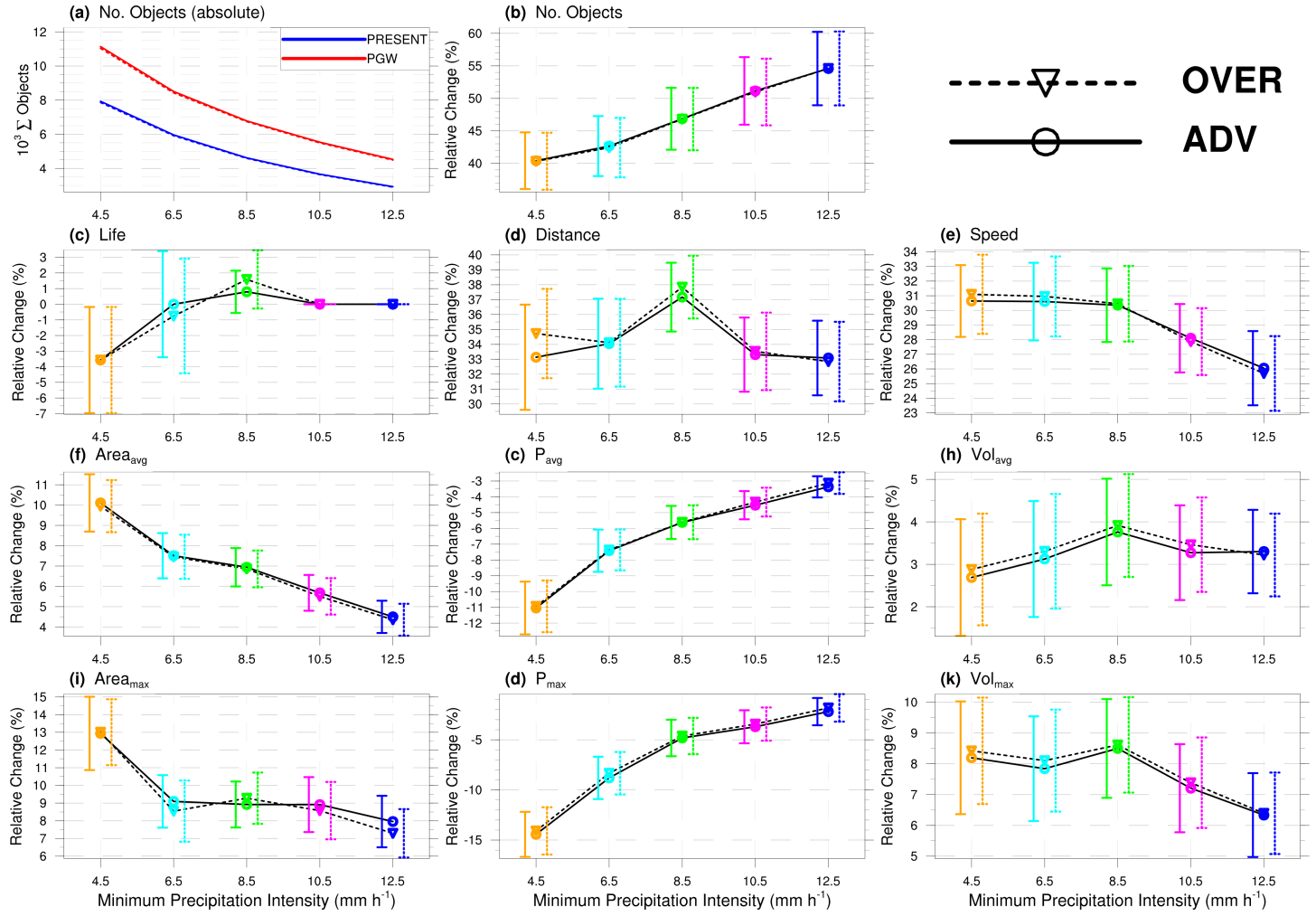


Figure S2: Climate-change signals of all object properties and N_{obj} as a function of the object's minimum-precipitation-intensity criterion P_{min} , for both algorithms. This plot includes the change signals for all object properties, and thus complements the change signals shown for selected properties in Fig. 4 of the main manuscript. Change signals which are different with statistical significance at the 0.95 level can be identified based on non-overlapping CIs (see Methods in main manuscript). P_{min} is shown as the equivalent hourly rate based on 5 min intensities. In panel (a), the absolute values for the number of objects are shown (i.e. the sample sizes). The absolute values underlying the change signals can be seen in Fig. S3

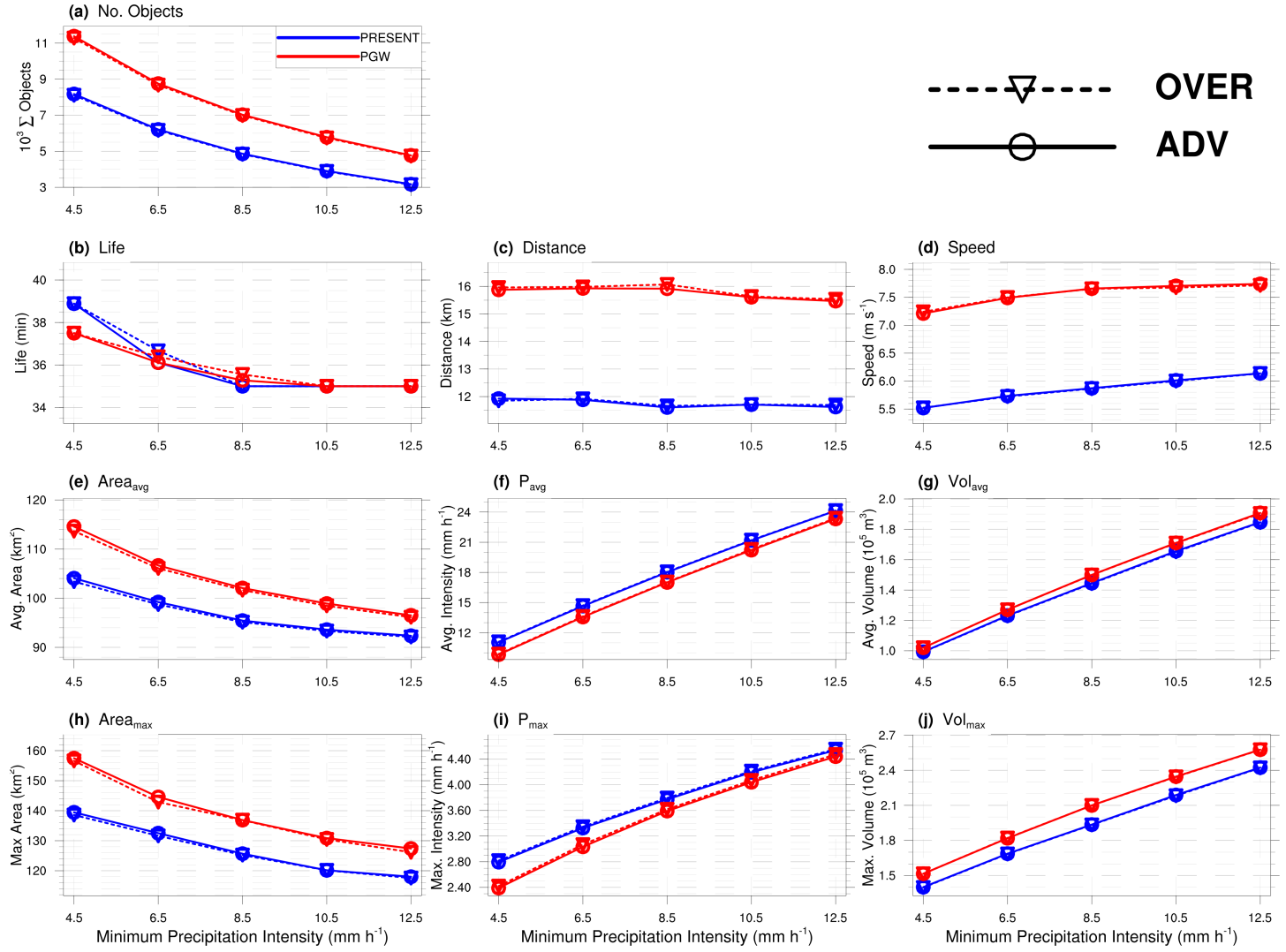


Figure S3: Different object properties in present and future climates as a function of the object's minimum-precipitation criterion P_{min} , for both algorithms. These are the absolute values underlying the change signals shown in Fig. 4 of the main manuscript and Fig. S2. P_{min} is shown as the equivalent hourly rate based on 5 min intensities.

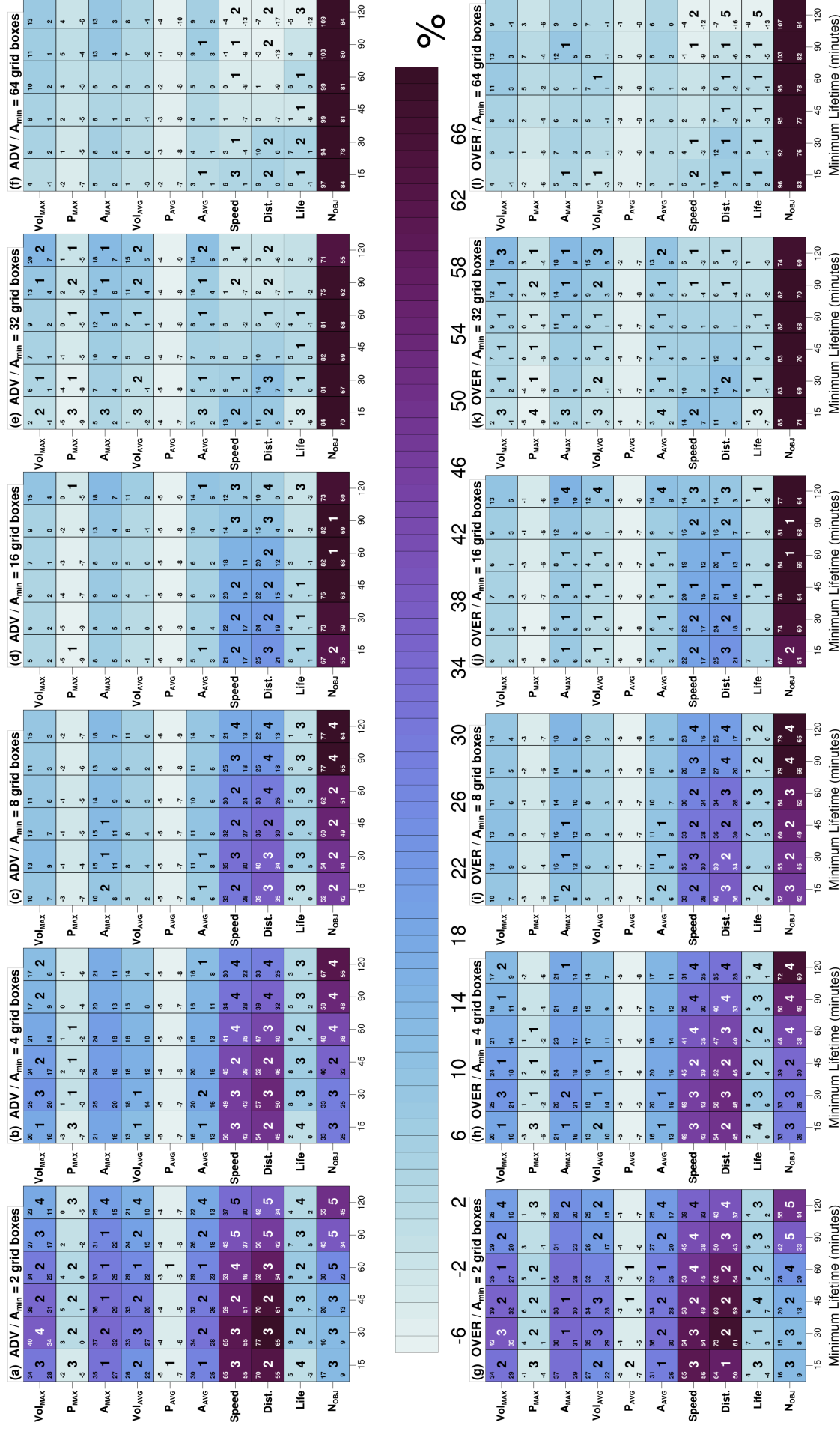


Figure S4: Climate-change signals of all object properties and N_{obj} , as a function of the object's minimum-lifetime criterion T_{min} , for both algorithms. Confidence intervals (computed as described in main manuscript) are given in the left-hand corners of each box. The number in the centre of each box (if present) denotes how many of the other T_{min} thresholds have change signals which are significantly different to the box in question (maximum = 5, $\alpha = 0.95$). For example, in the bottom row of panel (g) – OVER, $A_{min} = 2$ grid boxes, $N_{OBJ} -$ the value 3 is present at $T_{min} = 15$ minutes; this means 3 of the remaining 5 climate-changes signals (N_{OBJ} ; $T_{min} = 30$ -, 45-, 60-, 90-, 120- minutes) have a statistically significant difference to the box in question. There are no statistically significant differences between the algorithms. The results shown here include all six values of A_{min} , and thus complement the three values of A_{min} shown in the main manuscript.

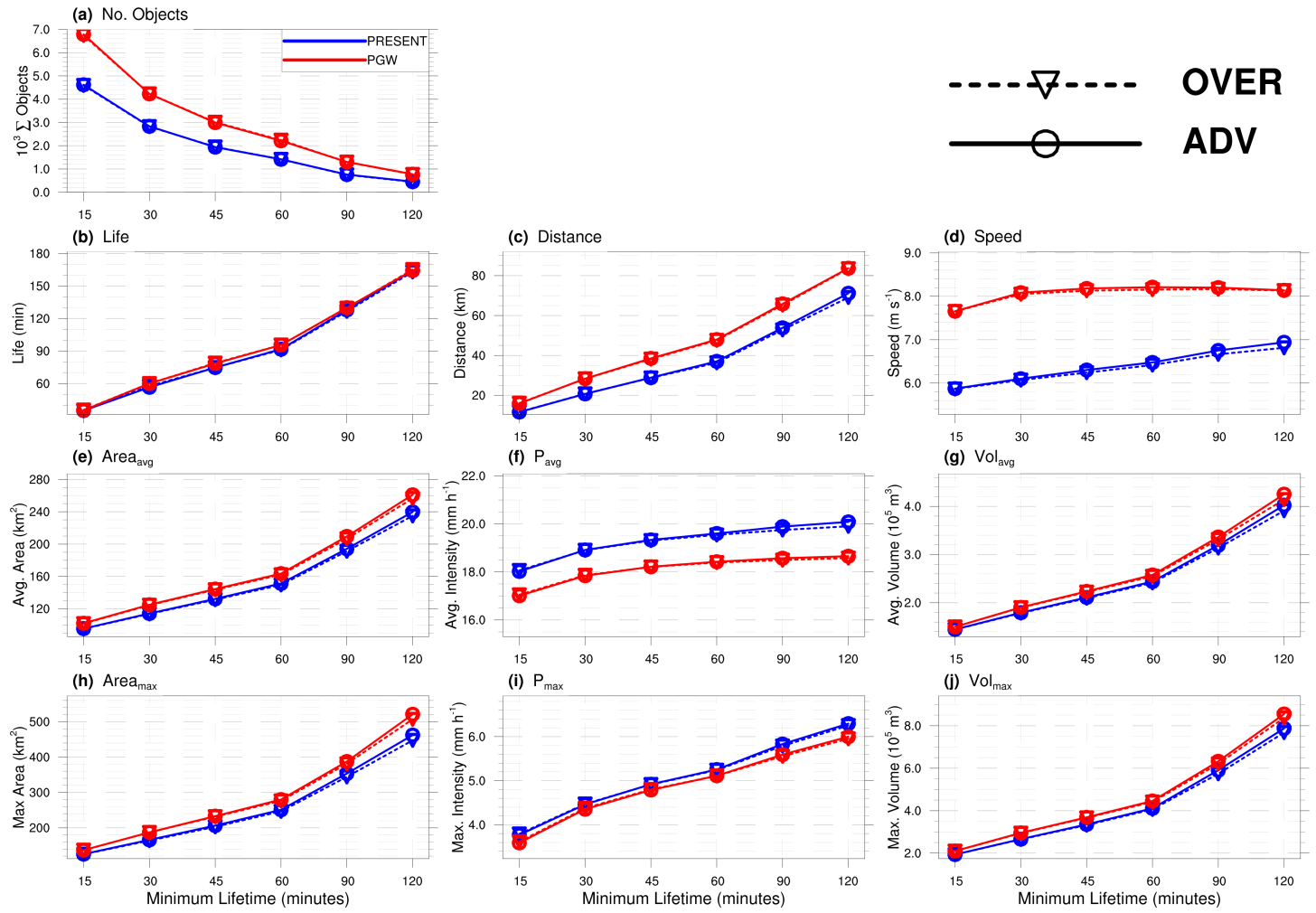


Figure S5: Different object properties, and N_{obj} , in present and future climates as a function of the object's minimum-lifetime criterion (T_{min}). In the figure, A_{min} has a value of 8 grid boxes and P_{min} a value of $8.5 mm h^{-1}$, i.e. the reference setup values. The figure thus shows the absolute values underlying the change signals in Fig. 4 (b, e) in the main manuscript and Fig. S4 (c, i) in this document.

2 Supporting discussion

2.1 Tests with other climate simulations

In Fig. S6, the reference settings have been used to repeat the tracking on a longer set of simulations, with both the ADV and OVER algorithms. These simulations comprise 30 summers from 1970-1999 and 2070-2099 under the RCP85 scenario, downscaled first over the EURO-CORDEX domain to 0.11° and then further to 0.02° over a smaller domain covering parts of western Germany, Benelux and parts of France. The simulations are described in the publications Meredith et al. (2018, 2019, 2021), where maps of the simulation domain can also be seen. The aim of this tracking, as mentioned in the main manuscript, is to see if the conclusion that the choice of tracking algorithm has no significant effect on the climate-change signal holds over a longer set of climate-change simulations. It could be speculated, for example, that the result in the main manuscript, i.e. that the tracking algorithm didn't affect the climate-change signal, is influenced by the particular set of weather situations which were present during the 14-day test period. If this were the case, then a longer set of climate simulations – which would naturally include a much larger set of weather situations – might be expected to reveal differences between the tracking algorithms. As can be seen in Fig. S6, in the climate-length simulations, the choice of tracking algorithm does not have a significant impact on the climate-change signal. The one exception is for the object-lifetime metric. It is worth commenting here that the object lifetime is the only discretized object property – in steps of 5 min. For this reason, small shifts in the distribution of object lifetimes can, when considering the median, have a large impact on the magnitude of the climate-change signal, thus producing apparently large differences in the climate-change signals between the two algorithms. Readers may additionally ask why these simulations weren't taken as the basis for the entire study. One reason is the computational expense associated with testing the different object definitions and algorithms at climate timescales (30 summers, present and future). The main reason, however, is that the simulation domain (which can be viewed in the aforementioned publications) is of suboptimal size for considering a diverse range of convective situations. Specifically, the domain is too small to consider larger convective systems whose spatial extent could easily exceed the width or length of the domain. Additionally, objects which travel a long distance may not complete their life cycles within the domain boundaries, thus making them ineligible for consideration. Convective objects which (i) are not fully captured within domain, (ii) begin their lives outside the domain, or (iii) end their lives outside the domain cannot be considered in the overall statistics because it is not possible to compute the object's properties when only data for a fraction of the object's life cycle or spatial extent is available. With the larger domain used in the main manuscript, this problem arises much less often.

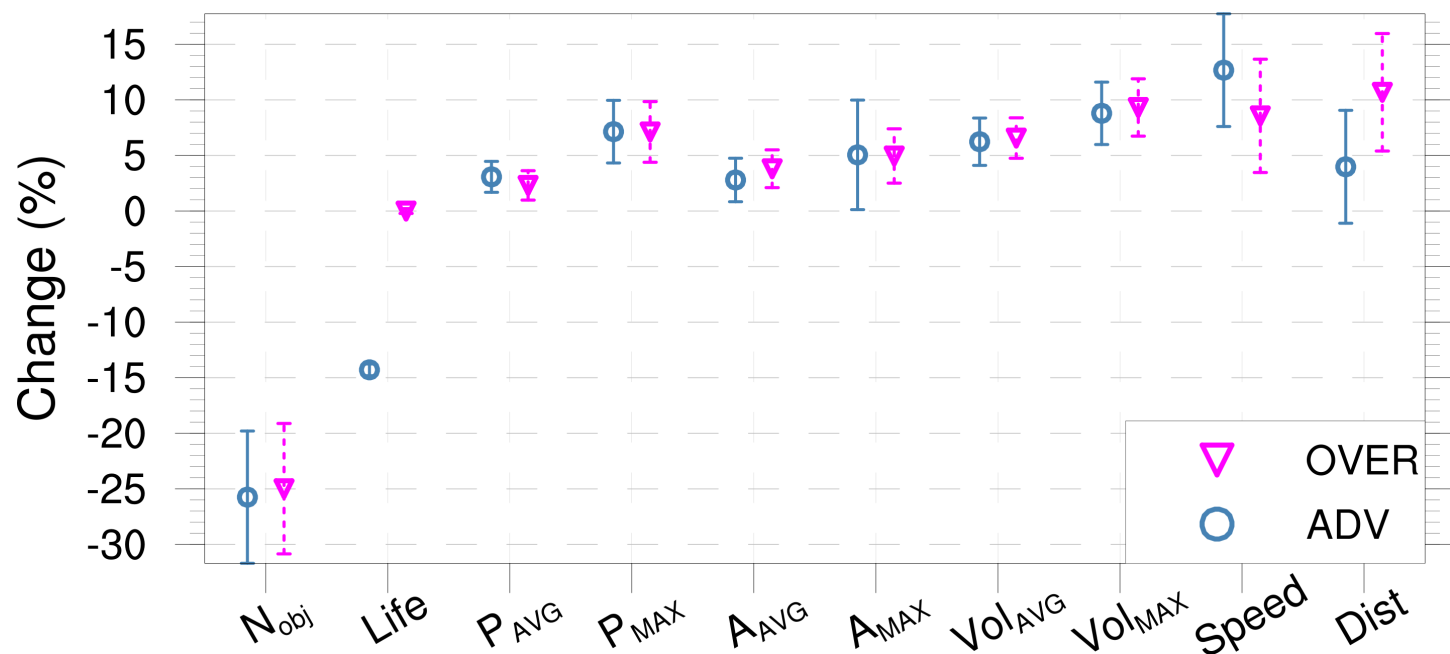


Figure S6: Climate-change signal for all object properties and N_{obj} based on the climate simulations used in Meredith et al. (2019). P_{min} and T_{min} take the reference values used in the present study. A_{min} closely matches the area of the reference A_{min} used in the present study, allowing for the fact that the simulations of Meredith et al. (2019) have a spatial resolution of 0.02° , as opposed to 0.025° in the present study.

2.2 Climate-change signals for higher quantiles

In Figs. S7-S9, the analysis of Figs. 3-5 from the main manuscript has been repeated, except using the 0.9-quantile instead of the median. It can be seen that the relationships between the different object properties and the varying thresholds are similar, leading to the same conclusions. Also apparent is that the confidence intervals of the climate-change signals sometimes widen, resulting in a reduced number of statistically significant differences. A final point of note is that the magnitudes and range of the climate-change signals are often quite different to those of the median, as shown in the main manuscript. This is to be expected, as it is well known that higher quantiles of precipitation do not necessarily respond to warming in the same way as the mean (or median). As discussed in the main manuscript, the magnitude of the detected climate-change signals is anyway not pertinent to the aim of the Results I section. Rather, the aim is assess *differences* in the climate-change signals and whether these are significant.

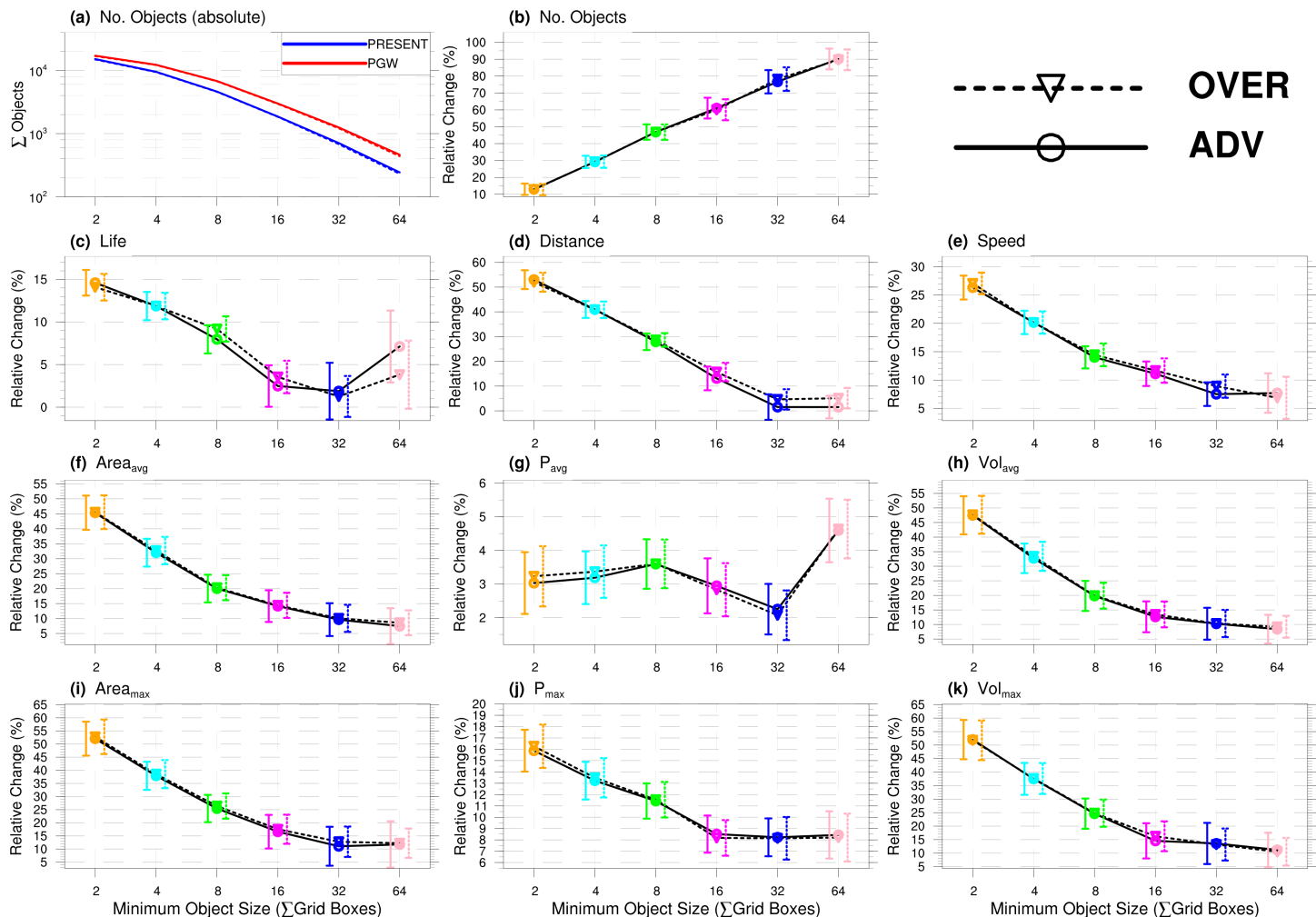


Figure S7: As in Fig. 3 of the main manuscript, i.e. varying A_{min} , except for the 0.9-quantile of each object property.

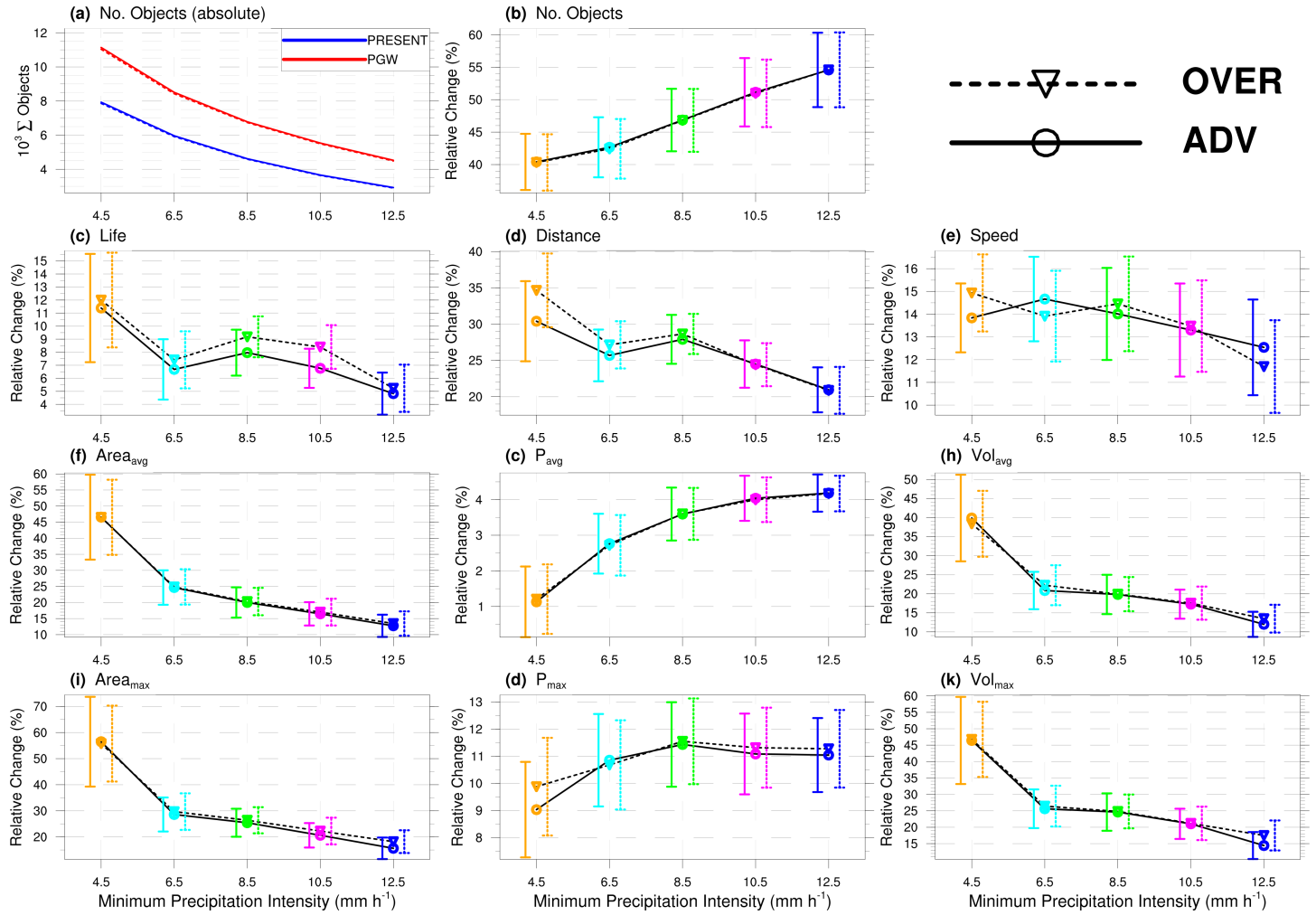


Figure S8: As in Fig. 4 of the main manuscript and Fig. S2, i.e. varying P_{min} , except for the 0.9-quantile of each object property.

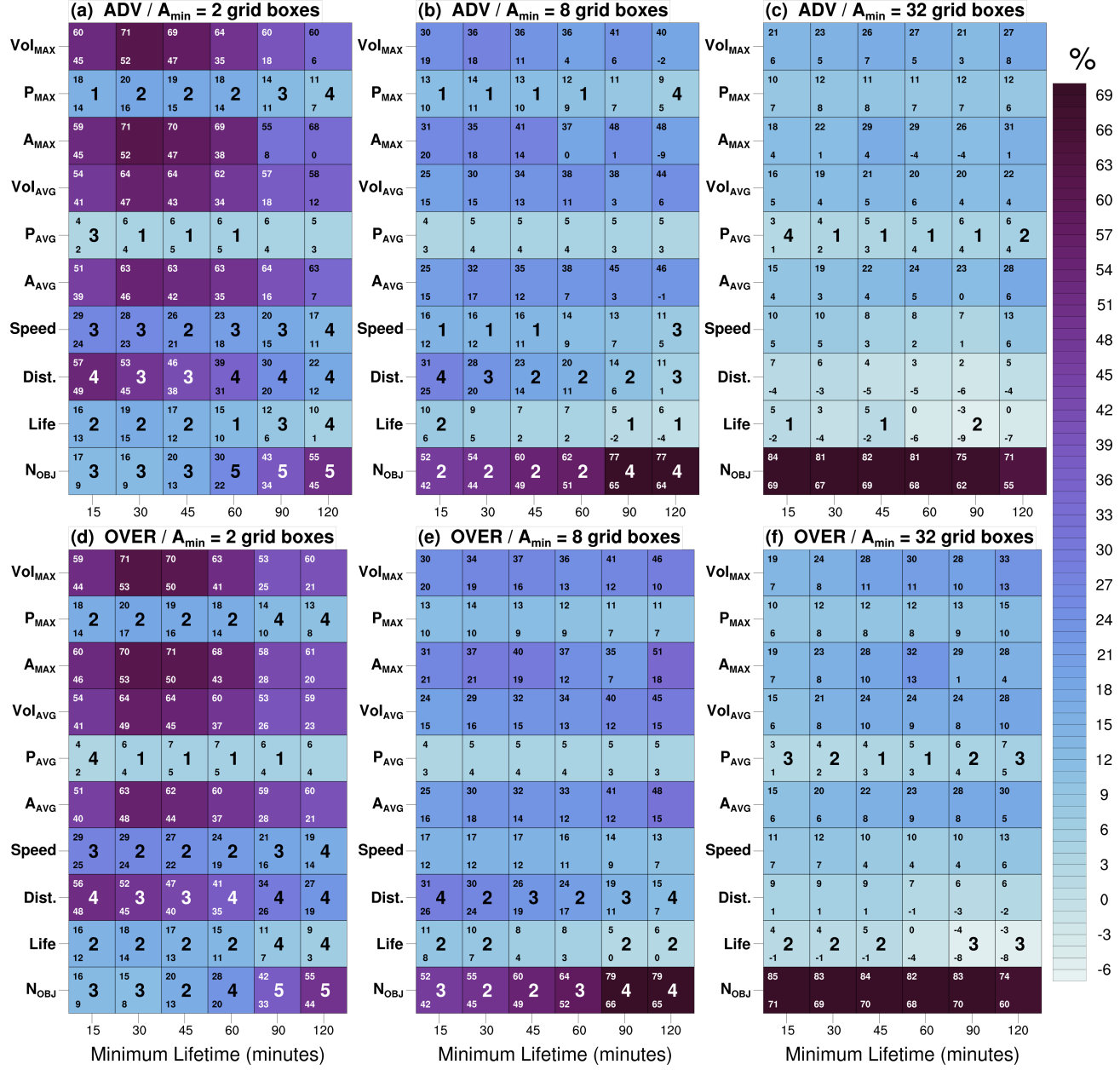


Figure S9: As in Fig. 5 of the main manuscript, i.e. varying T_{min} , except for the 0.9-quantile of each object property.

References

- E. P. Meredith, H. W. Rust, and U. Ulbrich. A classification algorithm for selective dynamical downscaling of precipitation extremes. *Hydrology and Earth System Sciences*, 22(8):4183–4200, 2018. doi: 10.5194/hess-22-4183-2018. URL <https://www.hydrol-earth-syst-sci.net/22/4183/2018/>.
- E. P. Meredith, U. Ulbrich, and H. W. Rust. The Diurnal Nature of Future Extreme Precipitation Intensification. *Geophysical Research Letters*, 46(13):7680–7689, 2019. doi: 10.1029/2019GL082385. URL <https://agupubs.onlinelibrary.wiley.com/doi/abs/10.1029/2019GL082385>.
- E. P. Meredith, U. Ulbrich, H. W. Rust, and H. Truhetz. Present and future diurnal hourly precipitation in 0.11° EURO-CORDEX models and at convection-permitting resolution. *Environmental Research Communications*, 3(5):055002, 2021. doi: 10.1088/2515-7620/abf15e.